Frink, Parikh and Pirzadeh and Liou and Steffen Jr. TVD Algorithms and Implicit Formulations Applied to the Euler Equations in 2D

EDISSON SÁVIO DE GÓES MACIEL

IEA – Aeronautical Engineering Division

ITA – Aeronautical Technological Institute

Praça Mal. Eduardo Gomes, 50 – Vila das Acácias – São José dos Campos – SP – 12228-900

BRAZIL

edissonsavio@yahoo.com.br   http://www.edissonsavio.eng.br

Abstract: - In this work, the Frink, Parikh and Pirzadeh and the Liou and Steffen Jr. schemes are implemented following a MUSCL approach, aiming to guarantee second order accuracy and to achieve TVD properties, and employing an implicit formulation to solve the Euler equations in the two-dimensional space. These schemes are implemented according to a finite volume formulation and using a structured spatial discretization. The former scheme is a flux difference splitting one, whereas the latter is a flux vector splitting scheme. The MUSCL approach employs five different types of nonlinear limiters, which assure TVD properties, namely: Van Leer limiter, Van Albada limiter, minmod limiter, Super Bee limiter and β-limiter. All variants of the MUSCL approach are second order accurate in space. The implicit schemes employ an ADI approximate factorization to solve implicitly the Euler equations. Explicit and implicit results are compared, as also the computational costs, trying to emphasize the advantages and disadvantages of each formulation. The schemes are accelerated to the steady state solution using a spatially variable time step, which has demonstrated effective gains in terms of convergence rate according to Maciel. The algorithms are applied to the solution of the physical problem of the moderate supersonic flow along a compression corner. The results have demonstrated that the most accurate solutions are obtained with the Frink, Parikh and Pirzadeh TVD scheme using the Van Leer and Super Bee nonlinear limiters, when implemented in its explicit version.

Key-Words: - Frink, Parikh and Pirzadeh algorithm, Liou and Steffen Jr. algorithm, MUSCL procedure, Implicit formulation, Flux difference splitting, Flux vector splitting, Euler equations, Two-dimensions.

1 Introduction

Conventional non-upwind algorithms have been used extensively to solve a wide variety of problems ([1]). Conventional algorithms are somewhat unreliable in the sense that for every different problem (and sometimes, every different case in the same class of problems) artificial dissipation terms must be specially tuned and judicially chosen for convergence. Also, complex problems with shocks and steep compression and expansion gradients may defy solution altogether.

Upwind schemes are in general more robust but are also more involved in their derivation and application. Some first order upwind schemes that have been applied to the Euler equations are:

[2] proposed a new scheme, unstructured and upwind, to the solution of the Euler equations. They tested the precision and the utility of this scheme in the analysis of the inviscid flows around two airplane configurations: one of transport configuration, with turbines under the wings, and the other of high speed civil configuration. Tests were accomplished at subsonic and transonic Mach numbers with the transport airplane and at transonic and low supersonic Mach numbers with the civil airplane, yielding good results.

[3] proposed a new flux vector splitting scheme. They declared that their scheme was simple and its accuracy was equivalent and, in some cases, better than the [4] scheme accuracy in the solutions of the Euler and the Navier-Stokes equations. The scheme was robust and converged solutions were obtained so fast as the [4] scheme. The authors proposed the approximated definition of an advection Mach number at the cell face, using its neighbor cell values via associated characteristic velocities. This interface Mach number was so used to determine the upwind extrapolation of the convective quantities.

Second order spatial accuracy can be achieved by introducing more upwind points or cells in the schemes. It has been noted that the projection stage, whereby the solution is projected in each cell face (i-1/2,j; i+1/2,j) on piecewise constant states, is the cause of the first order space accuracy of the [5] schemes ([6]). Hence, it is sufficient to modify the first projection stage without modifying the

Riemann solver, in order to generate higher spatial approximations. The state variables at the interfaces are thereby obtained from an extrapolation between neighboring cell averages. This method for the generation of second order upwind schemes based on variable extrapolation is often referred to in the literature as the MUSCL ("Monotone Upstream-centered Schemes for Conservation Laws") approach. The use of nonlinear limiters in such procedure, with the intention of restricting the amplitude of the gradients appearing in the solution, avoiding thus the formation of new extrema, allows that first order upwind schemes be transformed in TVD high resolution schemes with the appropriate definition of such nonlinear limiters, assuring monotone preserving and total variation diminishing methods.

Traditionally, implicit numerical methods have been praised for their improved stability and condemned for their large arithmetic operation counts ([7]). On the one hand, the slow convergence rate of explicit methods become they so unattractive to the solution of steady state problems due to the large number of iterations required to convergence, in spite of the reduced number of operation counts per time step in comparison with their implicit counterparts. Such problem is resulting from the limited stability region which such methods are subjected (the Courant condition). On the other hand, implicit schemes guarantee a larger stability region, which allows the use of CFL numbers above 1.0, and fast convergence to steady state conditions. Undoubtedly, the most significant efficiency achievement for multidimensional implicit methods was the introduction of the Alternating Direction Implicit (ADI) algorithms by [8-10], and fractional step algorithms by [11]. ADI approximate factorization methods consist in approximating the Left Hand Side (LHS) of the numerical scheme by the product of one-dimensional parcels, each one associated with a different spatial coordinate direction, which retract nearly the original implicit operator. These methods have been largely applied in the CFD community and, despite the fact of the error of the approximate factorization, it allows the use of large time steps, which results in significant gains in terms of convergence rate in relation to explicit methods.

In this work, the [2-3] schemes are implemented following a MUSCL approach, aiming to guarantee second order accuracy and to achieve TVD properties, and employing an implicit formulation to solve the Euler equations in the two-dimensional space. These schemes are implemented according to a finite volume formulation and using a structured spatial discretization. The former scheme is a flux difference splitting one, whereas the latter is a flux vector splitting scheme. The MUSCL approach employs five different types of nonlinear limiters, which assure TVD properties, namely: Van Leer limiter, Van Albada limiter, minmod limiter, Super Bee limiter and β-limiter. All variants of the MUSCL approach are second order accurate in space. The implicit schemes employ an ADI approximate factorization to solve implicitly the Euler equations. Explicit and implicit results are compared, as also the computational costs, trying to emphasize the advantages and disadvantages of each formulation. The schemes are accelerated to the steady state solution using a spatially variable time step, which has demonstrated effective gains in terms of convergence rate according to [12-13]. The algorithms are applied to the solution of the physical problem of the moderate supersonic flow along a compression corner. The results have demonstrated that the most accurate solutions are obtained with the [2] TVD scheme using the Van Leer nonlinear limiter to determine the best pressure distribution and the Super Bee nonlinear limiter to determine the best shock angle, when implemented in its explicit version.

2 Euler Equation

The fluid movement is described by the Euler equations, which express the conservation of mass, of the linear momentum and of the energy to an inviscid mean, heat non-conductor and compressible, in the absence of external forces. These equations can be represented, in the integral and conservative forms, to a finite volume formulation, by:

$$\partial/\partial t \int_V Q dV + \int_S \left[E n_x + F n_y \right] dS = 0 \,, \tag{1}$$

where Q is written to a Cartesian system, V is the cell volume, n_x and n_y are components of the normal unit vector to the flux face, S is the flux area, and E and F are components of the convective flux vector. The Q, E and F vectors are represented by:

$$Q = \left\{ \begin{array}{c} \rho \\ \rho u \\ \rho v \\ e \end{array} \right\}, \quad E = \left\{ \begin{array}{c} \rho u \\ \rho u^2 + p \\ \rho u v \\ (e+p)u \end{array} \right\} \text{ and } F = \left\{ \begin{array}{c} \rho v \\ \rho u v \\ \rho v^2 + p \\ (e+p)v \end{array} \right\}, \tag{2}$$

with ρ being the fluid density; u and v are Cartesian components of the velocity vector in the x and y directions, respectively; e is the total energy per unit volume of the fluid mean; and p is the static pressure of the fluid mean.

The Euler equations were nondimensionalized in relation to the freestream density, ρ_∞, and in relation to the freestream speed of sound, a_∞, to the studied problem in this work. The matrix system of the Euler equations is closed with the state equation of a perfect gas

$$p = (\gamma - 1)\left[e - 0.5\rho(u^2 + v^2)\right], \quad (3)$$

considering the ideal gas hypothesis. γ is the ratio of specific heats. The total enthalpy is determined by $H = (e + p)/\rho$.

3 Numerical Algorithms

The [2-3] first order schemes are described in details in [14-15]. In the present work, only the numerical flux vector of these schemes is presented:

3.1 [2] Algorithm

The [2] dissipation function can be written in terms of three flux components, each one associated with a distinct eigenvalue of the Euler equations:

$$D_{FPP} = \left|\Delta\tilde{F}_1\right| + \left|\Delta\tilde{F}_3\right| + \left|\Delta\tilde{F}_4\right|, \quad (4)$$

where:

$$\left|\Delta\tilde{F}_1\right| = \left|\tilde{\psi}_1\right| \left\{ \left(\Delta\rho - \frac{\Delta p}{\tilde{a}^2}\right) \begin{bmatrix} 1 \\ \tilde{u} \\ \tilde{v} \\ \dfrac{\tilde{u}^2 + \tilde{v}^2}{2} \end{bmatrix} + \tilde{\rho} \begin{bmatrix} 0 \\ \Delta u - n_x \Delta U \\ \Delta v - n_y \Delta U \\ \tilde{u}\Delta u + \tilde{v}\Delta v - \tilde{U}\Delta U \end{bmatrix} \right\}$$

$$\text{and} \quad \left|\Delta\tilde{F}_{3,4}\right| = \left|\tilde{\psi}_{3,4}\right| \left(\frac{\Delta p \pm \tilde{\rho}\tilde{a}\Delta U}{2\tilde{a}^2}\right) \begin{bmatrix} 1 \\ \tilde{u} \pm n_x \tilde{a} \\ \tilde{v} \pm n_y \tilde{a} \\ \tilde{H} \pm \tilde{U}\tilde{a} \end{bmatrix}, \quad (5)$$

with $\tilde{U} = \tilde{u}n_x + \tilde{v}n_y$; $\Delta U = n_x\Delta u + n_y\Delta v$; $\tilde{\rho}$, $\tilde{H}$, $\tilde{u}$ and $\tilde{v}$ are obtained from [4] average; $\tilde{a}$ is the speed of sound obtained from the averaged variables; and $\Delta(\cdot) = (\cdot)_{i+1,j} - (\cdot)_{i,j}$, to the (i+1/2,j) interface.

The present author suggests the implementation of an entropy function $\tilde{\psi}$ aiming to avoid zero contributions from the system's eigenvalues to the dissipation function of [2] algorithm. The entropy condition is implemented in the eigenvalues $\tilde{\lambda}_1 = \tilde{U}$, $\tilde{\lambda}_3 = \tilde{U} + \tilde{a}$ and $\tilde{\lambda}_4 = \tilde{U} - \tilde{a}$ of the following way:

$$\tilde{\psi}_l = \begin{cases} |Z_l|, & if \ |Z_l| \geq \varepsilon \\ 0.5\left(Z_l^2 + \varepsilon^2\right)/\varepsilon, & if \ |Z_l| < \varepsilon \end{cases}, \quad \text{with:}$$

$$Z_l = \tilde{\lambda}_l, \quad (6)$$

where the ε parameter assumes the value 0.01, recommended by the present author. In the original work of [2], the value of ε is equal to zero, which corresponds to the disregarding of the entropy condition. The convective numerical flux vector at the (i+1/2,j) interface is defined as:

$$F_{i+1/2,j}^{(l)} = \left(E_{\text{int}}^{(l)} n_{x_{i+1/2,j}} + F_{\text{int}}^{(l)} n_{y_{i+1/2,j}} - 0.5D_{FPP}^{(l)}\right)S\Big|_{i+1/2,j}, \quad (7)$$

with "l" varying from 1 to 4; $E_{\text{int}}^{(l)}$, $F_{\text{int}}^{(l)}$, S, n_x and n_y calculated as the same way as indicated in [14-16].

3.2 [3] Algorithm

The definition of the residual or the numerical flux vector of the [3] scheme proceeds as follows:

$$R_{i+1/2,j}^e = |S|\Big|_{i+1/2,j} \left\{ \frac{1}{2}M_{i+1/2,j} \left(\begin{bmatrix} \rho a \\ \rho a u \\ \rho a v \\ \rho a H \end{bmatrix}_L + \begin{bmatrix} \rho a \\ \rho a u \\ \rho a v \\ \rho a H \end{bmatrix}_R \right) \right.$$
$$\left. - \frac{1}{2}\phi_{i+1/2,j} \left(\begin{bmatrix} \rho a \\ \rho a u \\ \rho a v \\ \rho a H \end{bmatrix}_R - \begin{bmatrix} \rho a \\ \rho a u \\ \rho a v \\ \rho a H \end{bmatrix}_L \right) \right\} + \begin{Bmatrix} 0 \\ S_x p \\ S_y p \\ 0 \end{Bmatrix}_{i+1/2,j}, \quad (8)$$

with R [cell (i+1,j)] and L [cell (i,j)] related to right and left states; a is the speed of sound; S, S_x and S_y defining the flux area and its x and y components; these parameters are defined in [14-16]; the superscript "e" defines Euler equations; ϕ is the dissipation function which defines the particular numerical scheme. $M_{i+1/2,j}$ defines the advection Mach number at the (i+1/2,j) face of the (i,j) cell, which is calculated according to [3] as:

$$M_{i+1/2,j} = M_L^+ + M_R^-, \qquad (9)$$

where the separated Mach numbers $M^{+/-}$ are defined by the [17] formulas:

$$M^+ = \begin{bmatrix} M, & if\ M \geq 1; \\ 0.25(M+1)^2, & if\ |M| < 1; \quad and \\ 0, & if\ M \leq -1; \end{bmatrix}$$

$$M^- = \begin{bmatrix} 0, & if\ M \geq 1; \\ -0.25(M-1)^2, & if\ |M| < 1; \quad (10) \\ M, & if\ M \leq -1. \end{bmatrix}$$

M_L and M_R represent the Mach number associated with the left and right states, respectively. The Mach number at the cell interface to the calculation of the separated Mach numbers is defined by:

$$M = (S_x u + S_y v)/(|S|a); \qquad (11)$$

The pressure at the (i+1/2,j) face of the (i,j) cell is calculated by a similar way:

$$p_{i+1/2,j} = p_L^+ + p_R^-, \qquad (12)$$

with $p^{+/-}$ denoting the pressure separation defined according to the [17] formulas:

$$p^+ = \begin{bmatrix} p, & if\ M \geq 1; \\ 0.25p(M+1)^2(2-M), & if\ |M| < 1 \quad and \\ 0, & if\ M \leq -1; \end{bmatrix}$$

$$p^- = \begin{bmatrix} 0, & if\ M \geq 1; \\ 0.25p(M-1)^2(2+M), & if\ |M| < 1; \quad (13) \\ p, & if\ M \leq -1. \end{bmatrix}$$

The definition of the ϕ dissipation term which determines the [3] scheme, according to [18], is:

$$\phi_{i+1/2,j} = \phi_{i+1/2,j}^{LS} = |M_{i+1/2,j}|. \qquad (14)$$

4 MUSCL Procedure

Second order spatial accuracy can be achieved by introducing more upwind points or cells in the schemes. It has been noted that the projection stage, whereby the solution is projected in each cell face (i-1/2,j; i+1/2,j) on piecewise constant states, is the cause of the first order space accuracy of the [5] schemes ([6]). Hence, it is sufficient to modify the

first projection stage without modifying the Riemann solver, in order to generate higher spatial approximations. The state variables at the interfaces are thereby obtained from an extrapolation between neighboring cell averages. This method for the generation of second order upwind schemes based on variable extrapolation is often referred to in the literature as the MUSCL ("Monotone Upstream-centered Schemes for Conservation Laws") approach. The use of nonlinear limiters in such procedure, with the intention of restricting the amplitude of the gradients appearing in the solution, avoiding thus the formation of new extrema, allows that first order upwind schemes be transformed in TVD high resolution schemes with the appropriate definition of such nonlinear limiters, assuring monotone preserving and total variation diminishing methods. Details of the present implementation of the MUSCL procedure, as well the incorporation of TVD properties to the schemes, are found in [6]. The expressions to calculate de fluxes following a MUSCL procedure and the nonlinear flux limiter definitions employed in this work, which incorporates TVD properties, are defined as follows.

The conserved variables at the interface (i+1/2,j) can be considered as resulting from a combination of backward and forward extrapolations. To a linear one-sided extrapolation at the interface between the averaged values at the two upstream cells (i,j) and (i-1,j), one has:

$$Q_{i+1/2,j}^L = Q_{i,j} + \frac{\varepsilon}{2}(Q_{i,j} - Q_{i-1,j}), \text{ cell (i,j);} \quad (15)$$

$$Q_{i+1/2,j}^R = Q_{i+1,j} - \frac{\varepsilon}{2}(Q_{i+2,j} - Q_{i+1,j}), \text{ cell (i+1,j),} \qquad (16)$$

leading to a second order fully one-sided scheme. If the first order scheme is defined by the numerical flux

$$F_{i+1/2,j} = F(Q_{i,j}, Q_{i+1,j}) \qquad (17)$$

the second order space accurate numerical flux is obtained from

$$F_{i+1/2,j}^{(2)} = F(Q_{i+1/2,j}^L, Q_{i+1/2,j}^R). \qquad (18)$$

Higher order flux vector splitting or flux difference splitting methods, such as those studied in this work, are obtained from:

$$F_{i+1/2,j}^{(2)} = F^+(Q_{i+1/2,j}^L) + F^-(Q_{i+1/2,j}^R). \qquad (19)$$

All second order upwind schemes necessarily involve at least five mesh points or cells.

To reach high order solutions without oscillations around discontinuities, nonlinear limiters are employed, replacing the term ε in Eqs. (15) and (16) by these limiters at the left and at the right states of the flux interface. To define such limiters, it is necessary to calculate the ratio of consecutive variations of the conserved variables. These ratios are defined as follows:

$$r_{i-1/2,j}^+ = (Q_{i+1,j} - Q_{i,j})/(Q_{i,j} - Q_{i-1,j}) \quad \text{and}$$
$$r_{i+1/2,j}^+ = (Q_{i+2,j} - Q_{i+1,j})/(Q_{i+1,j} - Q_{i,j}), \quad (20)$$

where the nonlinear limiters at the left and at the right states of the flux interface are defined by $\Psi^L = \Psi(r_{i-1/2,j}^+)$ and $\Psi^R = \Psi(1/r_{i+1/2,j}^+)$. In this work, five options of nonlinear limiters were considered to the numerical experiments. These limiters are defined as follows:

$$\Psi_l^{VL}(r_l) = \frac{r_l + |r_l|}{1 + r_l}, \text{ [19] limiter;} \quad (21)$$

$$\Psi_l^{VA}(r_l) = \frac{r_l + r_l^2}{1 + r_l^2}, \text{ Van Albada limiter;} \quad (22)$$

$$\Psi_l^{MIN}(r_l) = signal_l MAX(0, MIN(|r_l|, signal_l)),$$
minmod limiter; (23)
$$\Psi_l^{SB}(r_l) = MAX(0, MIN(2r_l, 1), MIN(r_l, 2)),$$
"Super Bee" limiter, due to [20]; (24)
$$\Psi_l^{\beta-L}(r_l) = MAX(0, MIN(\beta r_l, 1), MIN(r_l, \beta)), \quad \beta\text{-}$$
limiter, (25)

with "l" varying from 1 to 4 (two-dimensional space), $signal_l$ being equal to 1.0 if $r_l \geq 0.0$ and -1.0 otherwise, r_l is the ratio of consecutive variations of the lth conserved variable and β is a parameter assuming values between 1.0 and 2.0, being 1.5 the value assumed in this work.

With the implementation of the numerical flux vectors following this MUSCL procedure, second order spatial accuracy and TVD properties are incorporated in the algorithms.

5 Implicit Formulations

All implicit schemes studied in this work used an ADI formulation to solve the algebraic nonlinear system of equations. Initially, the nonlinear system of equations is linearized considering the implicit operator evaluated at the time "n" and, posteriorly, the five-diagonal system of linear algebraic equations is factored in two three-diagonal systems of linear algebraic equations, each one associated with a particular spatial direction. Thomas algorithm is employed to solve these two three-diagonal systems. The implicit schemes studied in this work were only applicable to the solution of the Euler equations, which implies that only the convective contributions were considered in the RHS ("Right Hand Side") operator.

5.1 [2] TVD implicit scheme
The ADI form of the [2] TVD scheme is defined by the following two step algorithm:

$$\{I + \Delta t_{i,j}\Delta_\xi^- K_{i+1/2,j}^+ + \Delta t_{i,j}\Delta_\xi^+ K_{i+1/2,j}^-\}\Delta Q_{i,j}^* = [RHS_{(FPP)}]_{i,j}^n,$$
to the ξ direction; (26)
$$\{I + \Delta t_{i,j}\Delta_\eta^- J_{i,j+1/2}^+ + \Delta t_{i,j}\Delta_\eta^+ J_{i,j+1/2}^-\}\Delta Q_{i,j}^{n+1} = \Delta Q_{i,j}^*, \quad \text{to}$$
the η direction; (27)
$$Q_{i,j}^{n+1} = Q_{i,j}^n + \Delta Q_{i,j}^{n+1}, \quad (28)$$

where:

$$K_{i\pm1/2,j}^\pm = [R]_{i\pm1/2,j}^n \Omega_{i\pm1/2,j}^\pm [R^{-1}]_{i\pm1/2,j}^n;$$

$$J_{i,j\pm1/2}^\pm = [R]_{i,j\pm1/2}^n \Phi_{i,j\pm1/2}^\pm [R^{-1}]_{i,j\pm1/2}^n;$$

$$\Omega_{i\pm1/2,j}^\pm = diag\left[(\lambda_\xi^l)^\pm\right]_{i\pm1/2,j}^n;$$

$$\Phi_{i,j\pm1/2}^\pm = diag\left[(\lambda_\eta^l)^\pm\right]_{i,j\pm1/2}^n; \quad (29)$$

$$(\lambda_\xi^l)^\pm = 0.5(\lambda_\xi^l \pm |\lambda_\xi^l|); \quad (\lambda_\eta^l)^\pm = 0.5(\lambda_\eta^l \pm |\lambda_\eta^l|); \quad (30)$$

$$\Delta_\xi^- = (\cdot)_{i,j} - (\cdot)_{i-1,j};$$

$$\Delta_\xi^+ = (\cdot)_{i+1,j} - (\cdot)_{i,j};$$

$$\Delta_\eta^- = (\cdot)_{i,j} - (\cdot)_{i,j-1};$$

$$\Delta_\eta^+ = (\cdot)_{i,j+1} - (\cdot)_{i,j}. \quad (31)$$

In Equation (29), the R matrix is defined in [14-16]; $diag$ [·] is a diagonal matrix; in Eqs. (29) and (30), "l" assumes values from 1 to 4 and λ's are the eigenvalues of the Euler equations, defined in [15-16]. The matrix R^{-1} is defined in [21].

The $RHS_{(FPP)}$ operator required in Eq. (26) is defined as:

$$[RHS_{(FPP)}]_{i,j}^n = -\Delta t_{i,j}/V_{i,j}\left(F_{i+1/2,j}^{(FPP)} + F_{i-1/2,j}^{(FPP)} + F_{i,j+1/2}^{(FPP)} + F_{i,j-1/2}^{(FPP)}\right)^n,$$
(32)

with $F_{i+1/2,j}^{(FPP)}$ calculated according to Eq. (7) and the cell volume, $V_{i,j}$, defined in [14-15; 22]. This implementation is first order accurate in time due to the definition of Ω and of Φ, as reported in [23], but is second order accurate in space due to the RHS solution at the steady state, when a MUSCL procedure is employed.

5.2 [3] TVD implicit scheme
The ADI form of the [3] TVD scheme is defined by the following two step algorithm:

$$\left\{ I + \Delta t_{i,j}\Delta_\xi^- A_{i+1/2,j}^+ + \Delta t_{i,j}\Delta_\xi^+ A_{i+1/2,j}^- \right\}\Delta Q_{i,j}^* = \left[RHS_{(LS)} \right]_{i,j}^n,$$

to the ξ direction; (33)

$$\left\{ I + \Delta t_{i,j}\Delta_\eta^- B_{i,j+1/2}^+ + \Delta t_{i,j}\Delta_\eta^+ B_{i,j+1/2}^- \right\}\Delta Q_{i,j}^{n+1} = \Delta Q_{i,j}^*,$$

to the η direction; (34)

$$Q_{i,j}^{n+1} = Q_{i,j}^n + \Delta Q_{i,j}^{n+1}, \qquad (35)$$

where the matrices $A^\pm$ and $B^\pm$ are defined as:

$$A_{i\pm1/2,j}^\pm = [T]_{i\pm1/2,j}^n \Omega_{i\pm1/2,j}^\pm [T^{-1}]_{i\pm1/2,j}^n;$$

$$B_{i,j\pm1/2}^\pm = [T]_{i,j\pm1/2}^n \Phi_{i,j\pm1/2}^\pm [T^{-1}]_{i,j\pm1/2}^n; \qquad (36)$$

$$\Omega_{i\pm1/2,j}^\pm = diag\left[\left(\lambda_\xi^l\right)^\pm \right]_{i\pm1/2,j}^n;$$

$$\Phi_{i,j\pm1/2}^\pm = diag\left[\left(\lambda_\eta^l\right)^\pm \right]_{i,j\pm1/2}^n; \qquad (37)$$

The similarity transformation matrices, T and its inverse, are defined in [21]. The $RHS_{(LS)}$ operator required in Eq. (33) is defined to the [3] TVD scheme as:

$$\left[RHS_{(LS)} \right]_{i,j}^n = -\Delta t_{i,j}/V_{i,j}\left(R_{i+1/2,j}^{e(LS)} - R_{i-1/2,j}^{e(LS)} + R_{i,j+1/2}^{e(LS)} - R_{i,j-1/2}^{e(LS)} \right)^n, \qquad (38)$$

with $R_{i+1/2,j}^{e(LS)}$ calculated according to Eq. (8).

6 Spatially Variable Time Step
The basic idea of this procedure consists in keeping constant the CFL number in all calculation domain, allowing, hence, the use of appropriated time steps to each specific mesh region during the convergence process. Hence, according to the definition of the CFL number, it is possible to write:

$$\Delta t_{i,j} = CFL(\Delta s)_{i,j}/c_{i,j}, \qquad (39)$$

where CFL is the "Courant-Friedrichs-Lewy" number to provide numerical stability to the scheme; $c_{i,j} = \left[\left(u^2 + v^2\right)^{0.5} + a \right]_{i,j}$ is the maximum characteristic speed of information propagation in the calculation domain; and $(\Delta s)_{i,j}$ is a characteristic length of information transport. On a finite volume context, $(\Delta s)_{i,j}$ is chosen as the minor value found between the minor centroid distance, involving the (i,j) cell and a neighbour, and the minor cell side length.

7 Initial and Boundary Conditions

7.1 Initial condition
Values of freestream flow are adopted for all properties as initial condition, in the whole calculation domain, to the studied problem in this work ([24-25]):

$$Q_\infty = \left\{ 1 \quad M_\infty \cos\theta \quad M_\infty \sin\theta \quad \left[1/[\gamma(\gamma-1)] + 0.5M_\infty^2 \right] \right\}^T, \qquad (40)$$

where M_∞ represents the freestream Mach number and θ is the flow attack angle.

7.2 Boundary conditions
The boundary conditions are basically of three types: solid wall, entrance and exit. These conditions are implemented in special cells named ghost cells.

(a) Wall condition: This condition imposes the flow tangency at the solid wall. This condition is satisfied considering the wall tangent velocity component of the ghost volume as equals to the respective velocity component of its real neighbour cell. At the same way, the wall normal velocity component of the ghost cell is equalled in value, but with opposite signal, to the respective velocity component of the real neighbour cell.

The pressure gradient normal to the wall is assumed be equal to zero, following an inviscid formulation. The same hypothesis is applied to the temperature gradient normal to the wall, considering adiabatic wall. The ghost volume density and pressure are extrapolated from the respective values of the real neighbour volume (zero order extrapolation), with these two conditions. The total energy is obtained by the state equation of a perfect gas.

(b) Entrance condition:

(b.1) Subsonic flow: Three properties are specified and one is extrapolated, based on analysis of information propagation along characteristic directions in the calculation domain ([25]). In other words, three characteristic directions of information propagation point inward the computational domain and should be specified. Only the characteristic direction associated to the "(q_{normal}-a)" velocity cannot be specified and should be determined by interior information of the calculation domain. Pressure was the extrapolated variable to the present problem. Density and velocity components had their values determined by the freestream flow properties. The total energy per unity fluid volume is determined by the state equation of a perfect gas.

(b.2) Supersonic flow: All variables are fixed with their freestream flow values.

(c) Exit condition:

(c.1) Subsonic flow: Three characteristic directions of information propagation point outward the computational domain and should be extrapolated from interior information ([25]). The characteristic direction associated to the "(q_{normal}-a)" velocity should be specified because it penetrates the calculation domain. In this case, the ghost volume's pressure is specified by its freestream value. Density and velocity components are extrapolated and the total energy is obtained by the state equation of a perfect gas.

(c.2) Supersonic flow: All variables are extrapolated from the interior domain due to the fact that all four characteristic directions of information propagation of the Euler equations point outward the calculation domain and, with it, nothing can be fixed.

8 Results

Tests were performed in a microcomputer with processor INTEL CELERON, 1.5GHz of "clock", and 1.0Gbytes of RAM memory. Converged results occurred to 3 orders of reduction in the maximum residual value. As initial conditions, the entrance angle is equal to 0.0° and the freestream Mach number is equal to 3.0. The ratio of specific heats, γ, assumed the value 1.4. The reference to the limiters is abbreviated in this work: Van Leer limiter (VL), Van Albada limiter (VA), minmod limiter (Min), Super Bee limiter (SB) and β-limiter (BL). The explicit formulations of the [2-3] TVD schemes employ Runge-Kutta method and time splitting procedure, respectively, to time integration as described in [15].

8.1 Compression corner physical problem – Explicit simulations

The compression corner configuration is described in Fig. 1. The corner inclination angle is 10°. An algebraic mesh of 70x50 points or composed of 3,381 rectangular cells and 3,500 nodes was used and is shown in Fig. 2. The points are equally spaced in both directions.

Figure 1 : Compression corner configuration.
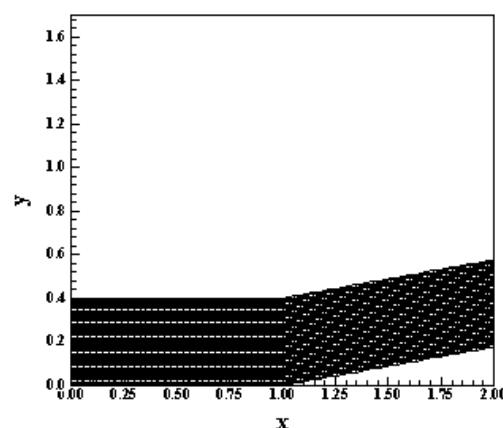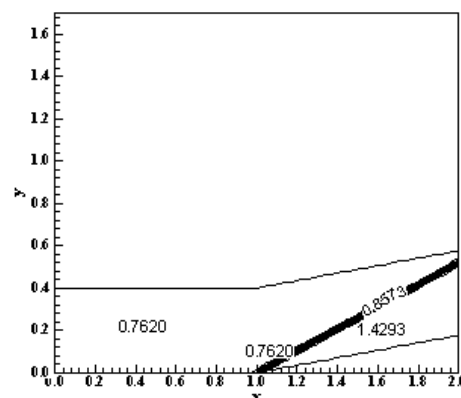

Figure 2 : Compression corner mesh.

Figure 3 : Pressure contours ([2]-VL).

Figures 3 to 7 exhibit the pressure contours obtained by the [2] TVD scheme in its five variants. As can be observed the most severe pressure after the shock is captured by the [2] TVD scheme using the SB variant, as also the

smallest shock wave thickness is captured by this limiter.
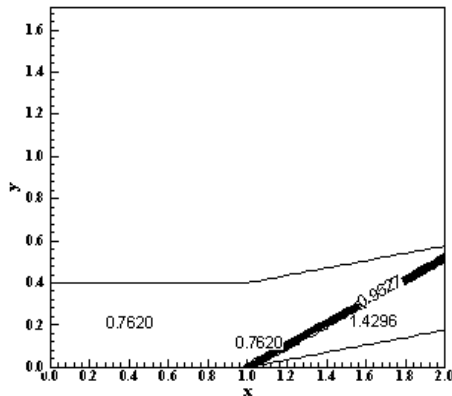

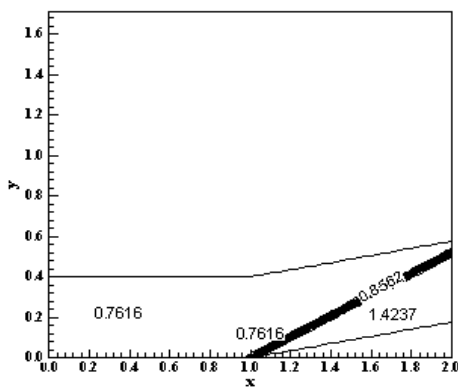Figure 4 : Pressure contours ([2]-VA).
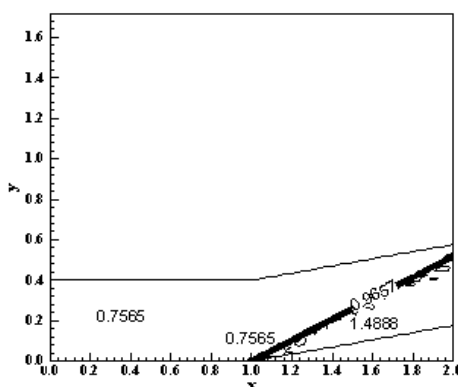

Figure 5 : Pressure contours ([2]-Min).

Figure 6 : Pressure contours ([2]-SB).

Figure 8 shows the wall pressure distributions obtained by all variants of the [2] TVD scheme. They are compared with the oblique shock wave theory. As can be observed, some solutions present oscillations at the compression corner, mainly the [2] TVD scheme using the SB limiter. Figure 9 exhibits the wall pressure distributions obtained by the [2] TVD scheme using VL, VA and Min limiters. As noted, no overshoot or undershoot are

observed in the solutions, presenting these ones a smooth behaviour. It is also possible to observe that the shock discontinuity is captured within three cells, which is a typical number of cells encountered in high resolution schemes to capture accurately shock waves. So the accuracy of the [2] TVD scheme with these three limiters is in accordance with typical results of current high resolution schemes. Figure 10 shows the wall pressure distributions obtained by the [2] TVD scheme using the SB and the BL limiters. The SB limiter yields oscillations along the shock plateau, but the shock is captured in three cells, as is the case with the BL limiter. By the results, the best solutions were obtained with VL, VA and Min limiters, which even capturing a less severe pressure after the shock, detect sharp and smooth pressure distributions at the corner wall.
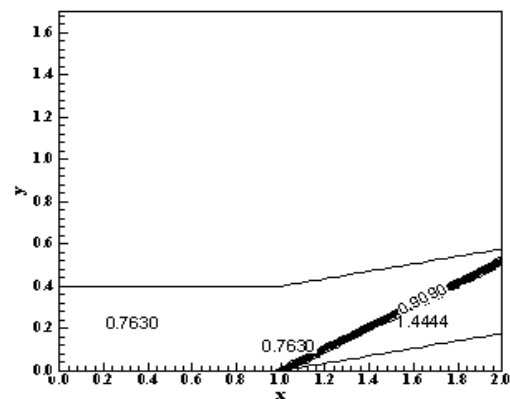
Figure 7 : Pressure contours ([2]-BL).
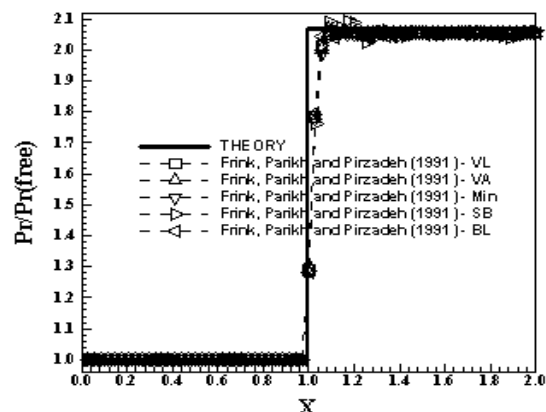
Figure 8 : Wall pressure distributions ([2]).

One way to quantitatively verify if the solutions generated by each scheme are satisfactory consists in determining the shock angle of the oblique shock wave, β, measured in relation to the initial direction of the flow field. [26] (pages 352 and 353) presents a diagram with values of the shock angle, β, to oblique shock waves. The value of this angle is

determined as function of the freestream Mach number and of the deflection angle of the flow after the shock wave, ϕ. To the compression corner problem, $\phi = 10º$ (ramp inclination angle) and the freestream Mach number is 3.0, resulting from this diagram a value to β equals to 27.5º.
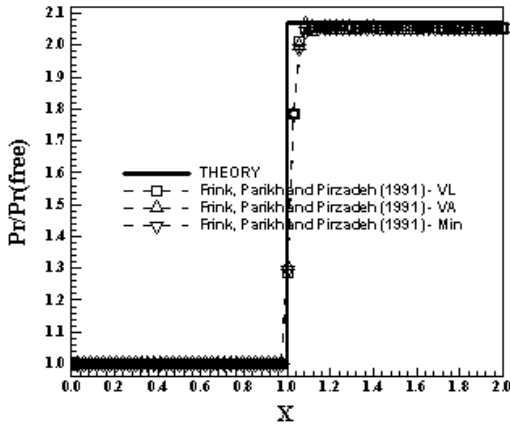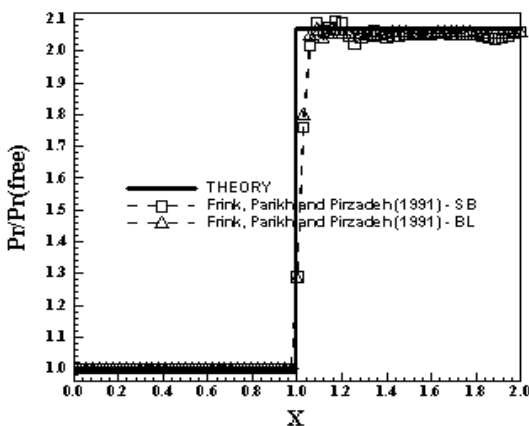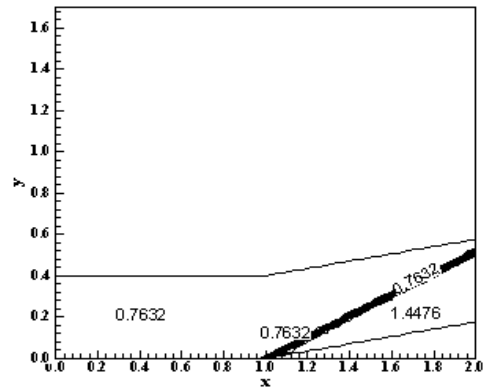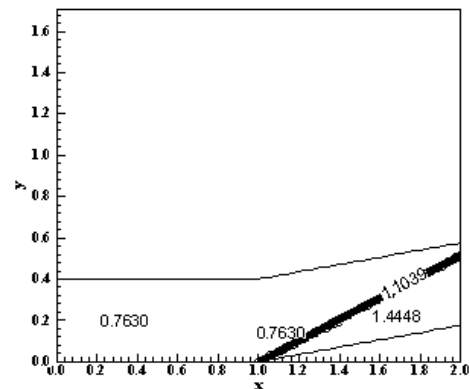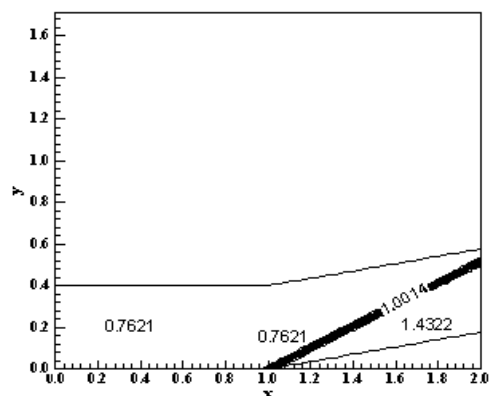

Figure 9 : Wall pressure distributions ([2]-1).

Figure 10 : Wall pressure distributions ([2]-2).

Table 1 : Shock angle and percentage errors ([2]/Explicit case).

Algorithm:	β (°):	Error (%):
[2] TVD – VL	28.0	1.82
[2] TVD – VA	27.6	0.36
[2] TVD – Min	28.2	2.55
[2] TVD – SB	27.5	0.00
[2]TVD – BL	28.4	3.27

Using a transfer in Figures 3 to 7, it is possible to obtain the values of β to each variant of the [2] TVD scheme, as well the respective errors, shown in Tab. 1. The [2] TVD scheme using the SB limiter has yielded the best result.

Figures 11 to 15 exhibit the pressure contours obtained by the [3] TVD scheme in its five variants. As can be observed the most severe pressure after the shock is captured by the [3] TVD scheme using the BL variant, although the smallest shock wave thickness is detected by the SB variant.

Figure 11 : Pressure contours ([3]-VL).

Figure 12 : Pressure contours ([3]-VA).

Figure 13 : Pressure contours ([3]-Min).

Figure 16 shows the wall pressure distributions obtained by all variants of the [3] TVD scheme. They are compared with the oblique shock wave theory. As can be observed, some solutions present oscillations at the compression corner, mainly the

[3] TVD scheme using the SB limiter, but they are in less amount than in the solutions of the variants of the [2] TVD scheme.
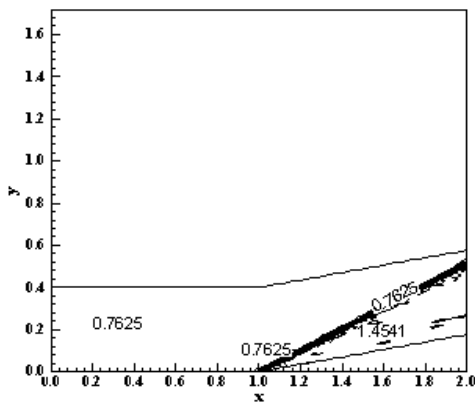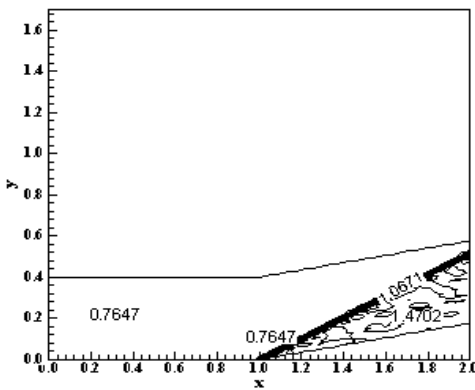

Figure 14 : Pressure contours ([3]-SB).

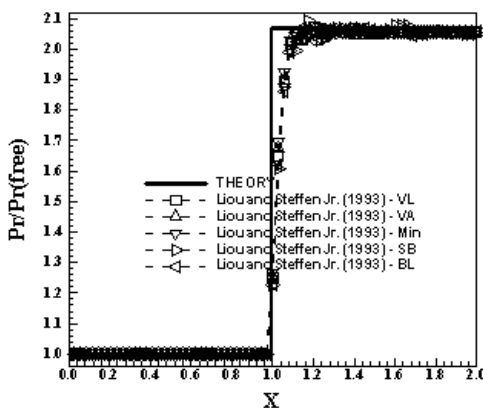Figure 15 : Pressure contours ([3]-BL).

Figure 16 : Wall pressure distributions ([3]).

Figure 17 exhibits the wall pressure distributions obtained by the [3] TVD scheme using VL, VA and Min limiters. As noted, no overshoot or undershoot are observed in the solutions, presenting these ones a smooth behavior. It is also possible to observe that the shock discontinuity is captured within four cells, which is a typical number of cells encountered in high resolution schemes to capture accurately shock

waves. So the accuracy of the [3] TVD scheme with these three limiters is in accordance with typical results of current high resolution schemes. Figure 18 shows the wall pressure distributions obtained by the [3] TVD scheme using the SB and the BL limiters. The SB limiter yields oscillations along the shock plateau, but the shock is also captured in four cells, as is the case with the BL limiter. By the results, the best solutions were obtained with VL, VA and Min limiters, which even capturing a less severe pressure after the shock, detect sharp and smooth pressure distributions at the corner wall.
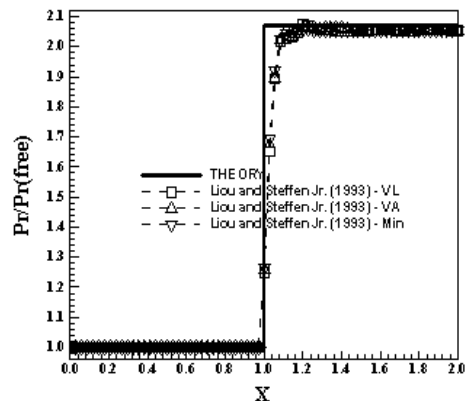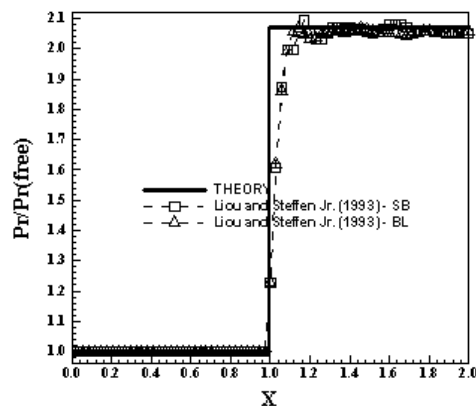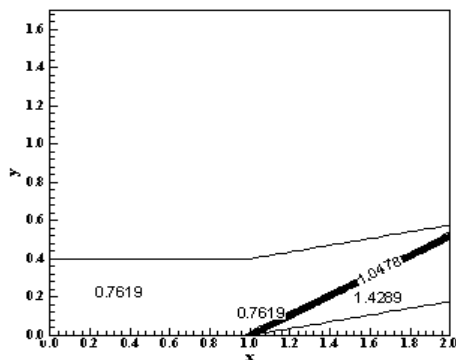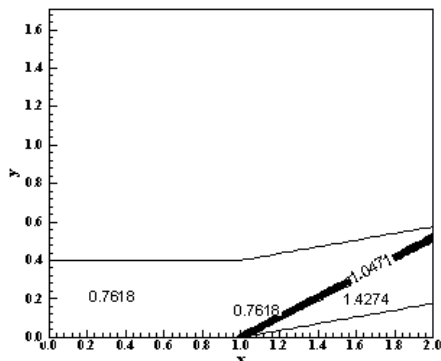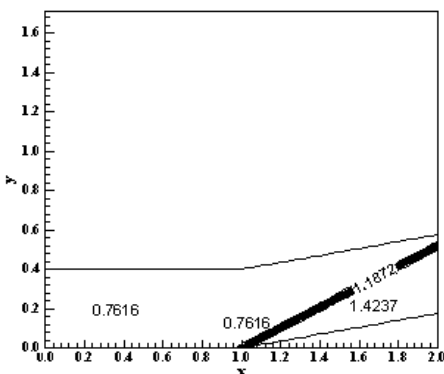

Figure 17 : Wall pressure distributions ([3]-1).

Figure 18 : Wall pressure distributions ([3]-2).

Table 2 : Shock angle and percentage errors ([3]/Explicit case).

Algorithm:	β (°):	Error (%):
[3] TVD – VL	27.6	0.36
[3] TVD – VA	27.6	0.36
[3] TVD – Min	27.9	1.45
[3] TVD – SB	27.5	0.00
[3] TVD – BL	27.5	0.00

Analysing the oblique shock wave angle, using a transfer in Figures 11 to 15, it is possible to obtain

the values of β to each variant of the [3] TVD scheme, as well the respective errors, shown in Tab. 2. The [3] TVD scheme using the SB and BL limiters have yielded the best results.

8.2 Compression corner physical problem – Implicit simulations

Figures 19 to 23 exhibit the pressure contours obtained by the [2] TVD scheme in its five variants. As can be observed the most severe pressure after the shock is captured by the [2] TVD scheme using the SB variant, as also the smallest shock wave thickness is captured by this limiter.

Figure 19 : Pressure contours ([2]-VL).

Figure 20 : Pressure contours ([2]-VA).
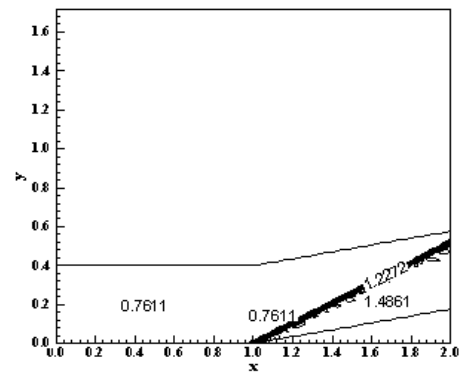

Figure 21 : Pressure contours ([2]-Min).

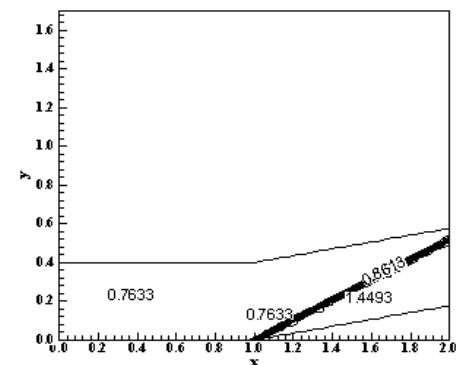Figure 22 : Pressure contours ([2]-SB).

Figure 23 : Pressure contours ([2]-BL).

Figure 24 shows the wall pressure distributions obtained by all variants of the [2] TVD scheme. They are compared with the oblique shock wave theory. As noted, some solutions present oscillations at the compression corner, mainly the [2] TVD scheme using the SB limiter.
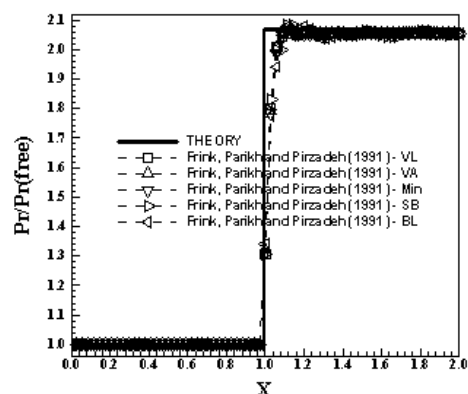

Figure 24 : Wall pressure distributions ([2]).

Figure 25 exhibits the wall pressure distributions obtained by the [2] TVD scheme using VL, VA and Min limiters. No overshoot or undershoot are observed in the solutions, presenting these ones a smooth behaviour. It is also possible to note that the shock discontinuity is captured in three cells, which

is also a typical number of cells encountered in high resolution schemes to capture accurately shock waves. Hence, as in the explicit case, the accuracy of the [2] TVD scheme with these three limiters is in accordance with typical results of current high resolution schemes. Figure 26 shows the wall pressure distributions obtained by the [2] TVD scheme using the SB and BL limiters. The SB limiter yields oscillations along the shock plateau, but the shock is captured in three cells, as is the case with the BL limiter. By the results, the best solutions were obtained with VL, VA and Min limiters, which even capturing a less severe pressure after the shock, detect sharp and smooth pressure distributions at the corner wall.

Analysing the oblique shock wave angle, using a transfer in Figures 19 to 23, it is possible to obtain the values of β to each variant of the [2] TVD scheme, as well the respective errors, shown in Tab. 3. The [2] TVD scheme using the VA limiter has yielded the best result.

Figures 27 to 31 exhibit the pressure contours obtained by the [3] TVD scheme in its five variants to the implicit case. As observed, the most severe pressure after the shock is captured by the [3] TVD scheme using the BL variant, although the smallest shock wave thickness is due to the SB limiter.
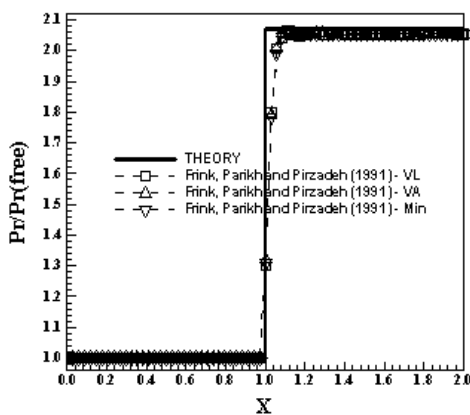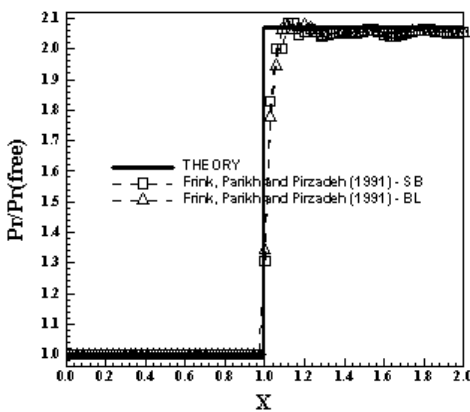

Figure 25 : Wall pressure distributions ([2]-1).

Figure 26 : Wall pressure distributions ([2]-2).

Table 3 : Shock angle and percentage errors ([2]/Implicit case).

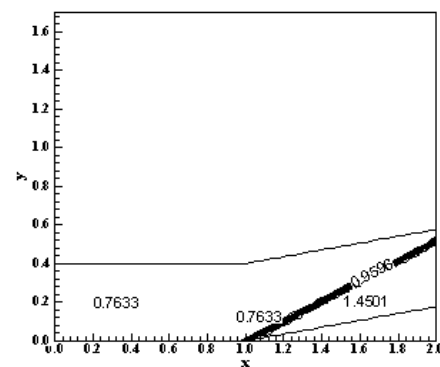| Algorithm:	β (°):	Error (%):
[2] TVD – VL	28.0	1.82
[2] TVD – VA	27.9	1.45
[2] TVD – Min	28.4	3.27
[2] TVD – SB	28.0	1.82
[2] TVD – BL	28.0	1.82

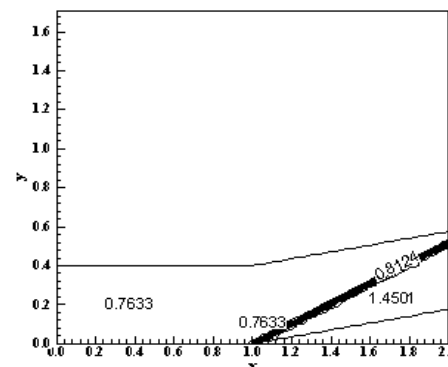Figure 27 : Pressure contours ([3]-VL).
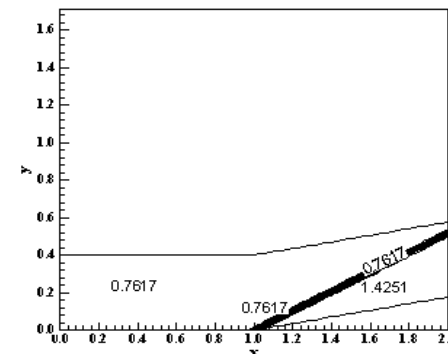

Figure 28 : Pressure contours ([3]-VA).

Figure 29 : Pressure contours ([3]-Min).

Figure 32 shows the wall pressure distributions obtained by all variants of the [3] TVD scheme.

They are compared with the oblique shock wave theory. As noted, some solutions present oscillations at the compression corner, mainly the [3] TVD scheme using the SB limiter. Figure 33 exhibits the wall pressure distributions obtained by the [3] TVD scheme using VL, VA and Min limiters.
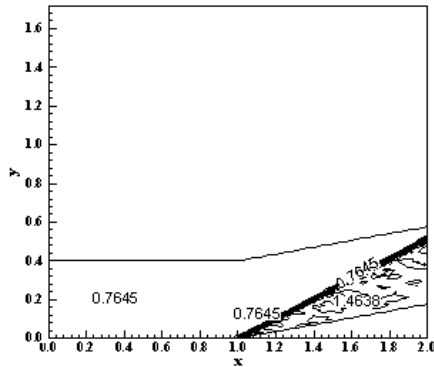

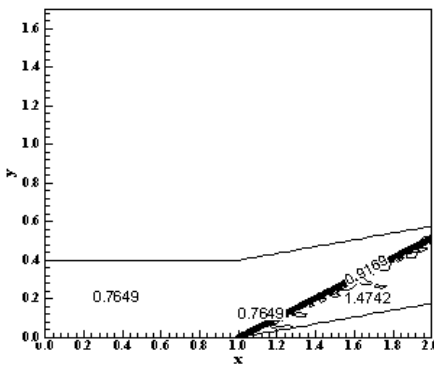Figure 30 : Pressure contours ([3]-SB).
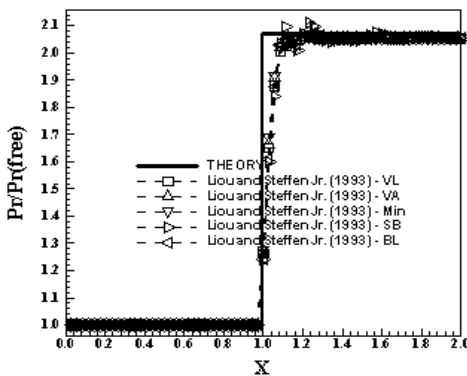

Figure 31 : Pressure contours ([3]-BL).

Figure 32 : Wall pressure distributions ([3]).

As observed, no overshoot or undershoot are noted in the solutions, presenting these ones a smooth behaviour. It is also possible to observe that the shock discontinuity is captured in four cells, a typical number of cells to high resolution schemes capture accurately shock waves. Hence, the accuracy of the [3] TVD scheme with these three

limiters is in accordance with typical results of current high resolution schemes. Figure 34 shows the wall pressure distributions obtained by the [3] TVD scheme using SB and BL limiters. The SB limiter yields oscillations along the shock plateau, but the shock discontinuity is also captured within four cells, as is the case with the BL limiter. By the results, the best solutions were obtained with VL, VA and Min limiters, which even capturing a less severe pressure after the shock, detect sharp and smooth pressure distributions at the corner wall.
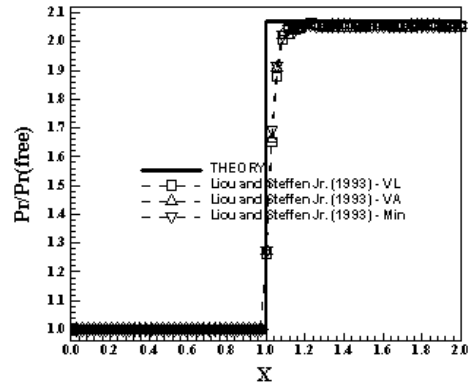
Figure 33 : Wall pressure distributions ([3]-1).
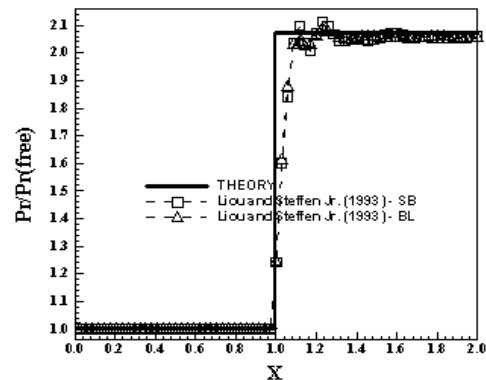
Figure 34 : Wall pressure distributions ([3]-2).

Table 4 : Shock angle and percentage errors ([3]/Implicit case).

Algorithm:	β (°):	Error (%):
[3] TVD – VL	27.4	0.36
[3] TVD – VA	28.0	1.82
[3] TVD – Min	28.0	1.82
[3] TVD – SB	27.8	1.09
[3] TVD – BL	27.9	1.45

Analysing the oblique shock wave angle, using a transfer in Figures 27 to 31, it is possible to obtain the values of β to each variant of the [3] TVD scheme, as well the respective errors, shown in Tab.

4. The [3] TVD scheme using the VL limiter has yielded the best result.

8.3 Explicit versus implicit comparisons

Figure 35 exhibits the best wall pressure distributions obtained by the variants of the [2] TVD scheme and by the variants of the [3] TVD scheme in their explicit versions.

Figure 35 : Wall pressure distributions (Exp).

Figure 36 : Wall pressure distributions (Imp).
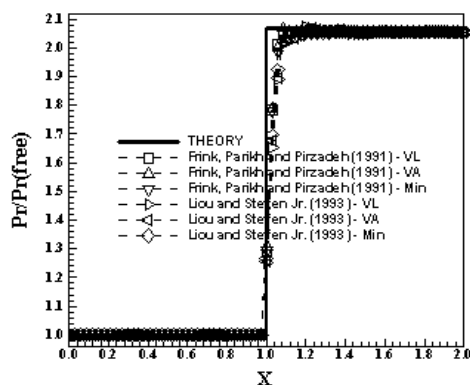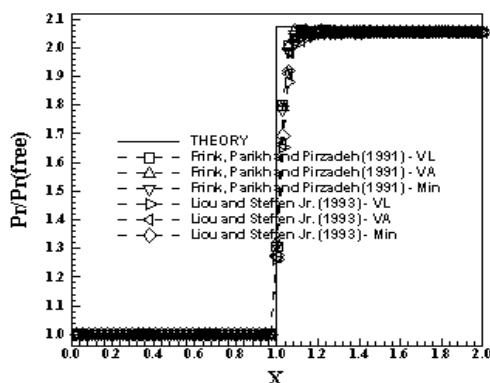
Only the solutions obtained with the VL, VA and Min limiters of each scheme are presented. The [2] TVD variants and the [3] TVD variants are in close agreement. The [2] solutions in the explicit results capture the shock discontinuity in three cells, whereas the [3] solutions in four cells. The best wall pressure distribution in this comparison was obtained by the [2] TVD scheme using VL limiter. Figure 36 shows the best wall pressure distributions obtained by the variants of the [2] TVD scheme and by the variants of the [3] TVD scheme in their implicit versions. Again, only the solutions obtained with the VL, VA and Min limiters of each scheme are presented. Again, the [2] solutions in the implicit results capture the shock discontinuity in three cells, whereas the [3] solutions in four cells. The best wall pressure distribution in this comparison was obtained again by the [2] TVD scheme using now the Min limiter.

Table 5 presents the best values to the shock angle obtained by the variants of the [2] TVD scheme and by the variants of the [3] TVD scheme. As can be observed, the best results are obtained with the [2] TVD scheme using SB (explicit case) limiter and with the [3] TVD scheme using SB and BL (explicit case) limiters. As can be concluded, the explicit results were better than the implicit ones. The [2] TVD scheme using VL and Min limiters yielded the best wall pressure distribution in both explicit and implicit cases, respectively, and the best shock angle value in the explicit case using SB limiter. Hence, the [2] TVD scheme using VL and SB limiters, considering the explicit case, are the best choices in this study.

Table 5 : Shock angle and percentage errors (Explicit and Implicit Results).

Algorithm:	β (°):	Error (%):
[2] TVD – SB – Explicit	27.5	0.00
[3] TVD – SB – Explicit	27.5	0.00
[3] TVD – BL – Explicit	27.5	0.00

Table 6 : Comparison between explicit and implicit computational costs.

Scheme:	Explicit Cost[1]:	Implicit Cost[1]:	Increase (%):
[2] TVD – VL	0.0000827	0.0000507	-63.12
[2] TVD – VA	0.0000857	0.0000510	-68.04
[2] TVD – Min	0.0000859	0.0000504	-70.44
[2] TVD – SB	0.0000820	0.0000504	-62.70
[2] TVD – BL	0.0000817	0.0000506	-61.46
[3] TVD – VL	0.0000059	0.0000347	488.14
[3] TVD – VA	0.0000061	0.0000349	472.13
[3] TVD – Min	0.0000058	0.0000343	491.38
[3] TVD – SB	0.0000058	0.0000345	494.83
[3] TVD – BL	0.0000058	0.0000344	493.10

[1]: Measured in seconds/per cell/per iteration.

Table 6 presents the computational costs of the variants of the [2] TVD scheme and of the variants of the [3] TVD scheme, as also the respective percentage increase in the computational cost when passing from the explicit version to the implicit version. As can be observed the cheapest scheme, in its explicit version, is due to [3] TVD scheme using Min, SB or BL limiters and the most expensive is due to the [2] TVD scheme using Min limiter. The increase in computational cost involving these two schemes is 1,381.0%; in other words, the [3] TVD scheme using Min, SB or BL limiter is 1,381.0% cheaper than the Min variant of the [2] TVD scheme. In the implicit case, the cheapest scheme is

the [3] TVD scheme using Min limiter, whereas the most expensive is due to the [2] TVD scheme using VA limiter. The increase in computational cost when passing from the [3] TVD scheme using Min limiter to the [2] TVD scheme using VA limiter is 48.7%.

Another important consideration taking into account Tab. 6 is the negative values to the increase of the computational cost involving the variants of the [2] TVD scheme. It means that the implicit costs were smaller than the explicit ones. It can be explained because the explicit numerical scheme of [2] employs a Runge-Kutta method of five stages to perform the time integration, which severely damages the explicit computational costs. On the other hand, the implicit implementation of this scheme is well optimized, which reduces efficiently the computational costs. Therefore, the implicit costs of the variants of the numerical scheme of [2] are smaller than the explicit ones, resulting in the decrease of the computational cost when passing from explicit to implicit formulation. In the [3] case, the explicit integration employs a time splitting procedure, which is not expensive.

9 Conclusions

In the present work, first part of this study, the theories involving the extension of the first order versions of the numerical schemes of [2] and of [3] to second order, incorporating hence TVD properties through a MUSCL approach, and the implicit numerical implementation of these second order schemes are detailed. The schemes are implemented on a finite volume context, using a structured spatial discretization. First order time integrations like ADI approximate factorization are programmed. The Euler equations in conservation and integral forms, in two-dimensions, are solved. The steady state physical problem of the moderate supersonic flow along a compression corner is studied and compared with theoretical results. A spatially variable time step procedure is also implemented aiming to accelerate the convergence to the steady solution. The gains in convergence with this procedure were demonstrated in [12-13].

The results have demonstrated that the most accurate solutions are obtained with the [2] TVD scheme using VL and Min nonlinear limiters to obtain the best pressure distributions in the explicit and implicit cases, respectively, and using the SB nonlinear limiter, in the explicit case, to obtain the best value to the shock angle of the oblique shock wave. The best results in the capture of the shock discontinuity in the corner problem were obtained

by the VL, VA and Min variants of the [2] and of the [3] TVD schemes, without present oscillations, under- or overshoots. This behaviour was observed in the explicit and implicit simulations. Both explicit and implicit versions of the [2] TVD scheme capture the shock discontinuity in three cells, whereas the [3] TVD versions capture in four cells. The best wall pressure distribution obtained in both explicit and implicit cases are due to [2] TVD scheme using VL and Min limiter, respectively. The shock angle was correctly estimated by the [2] TVD scheme using SB (explicit case) limiter. The [3] TVD scheme also captures correctly the shock angle using SB and BL limiters in the explicit case. In other words, the explicit formulation provides the best results. Hence, as the explicit results are better than the implicit ones and taking into account that the [2] TVD scheme using SB limiter yields the best shock angle value, while the best wall pressure distributions is obtained using VL limiter, this scheme with these variants are the best choices in this study. The second order MUSCL approach provides solutions free of oscillations as using the VL, VA and Min limiters, highlighting its TVD properties.

The cheapest scheme, in its explicit version, is due to [3] TVD scheme using Min, SB or BL limiters and the most expensive are due to [2] TVD scheme using Min limiter. The increase in computational cost involving these variants is 1,381.0%. In the implicit case, the cheapest scheme is the [3] TVD scheme using Min limiter, whereas the most expensive is due to [2] TVD scheme using VA limiter. The increase in computational cost in this case is 48.7%.

10 Acknowledgments

References:
[1] P. Kutler, Computation of Three-Dimensional, Inviscid Supersonic Flows, *Lecture Notes in Physics*, Vol. 41, 1975, pp. 287-374.
[2] N. T. Frink, P. Parikh, and S. Pirzadeh, Aerodynamic Analysis of Complex Configurations Using Unstructured Grids, 1991, *AIAA 91-3292-CP*.

[3] M. Liou, and Steffen Jr., C. J., A New Flux Splitting Scheme, *Journal of Computational Physics*, Vol. 107, 1993, pp. 23-39.

[4] P. L. Roe, Approximate Riemann Solvers, Parameter Vectors, and Difference Schemes, *Journal of Computational Physics*, Vol. 43, 1981, pp. 357–372.

[5] S. K. Godunov, A Difference Scheme for Numerical Computation of Discontinuous Solution of Hydrodynamic Equations, *Math. Sbornik*, Vol. 47, 1959, pp. 271-306.

[6] C. Hirsch, *Numerical Computation of Internal and External Flows – Computational Methods for Inviscid and Viscous Flows*, John Wiley & Sons Ltd, 691p., 1990.

[7] R. M. Beam, and R. F. Warming, An Implicit Factored Scheme for the Compressible Navier-Stokes Equations, *AIAA Journal*, Vol. 16, No. 4, 1978, pp. 393-402.

[8] J. Douglas, On the Numerical Integration of $u_{xx}+u_{yy}=u_t$ by Implicit Methods, *Journal of the Society of Industrial and Applied Mathematics*, Vol. 3, 1955, pp. 42-65.

[9] D. W. Peaceman, and H. H. Rachford, The Numerical Solution of Parabolic and Elliptic Differential Equations, *Journal of the Society of Industrial and Applied Mathematics*, Vol. 3, 1955, pp. 28-41.

[10] J. Douglas, and J. E. Gunn, A General Formulation of Alternating Direction Methods, *Numerische Mathematiks*, Vol. 6, 1964, pp. 428-453.

[11] N. N. Yanenko, *The Method of Fractional Steps*, Springer Verlag, N.Y., EUA, 1971.

[12] E. S. G. Maciel, Analysis of Convergence Acceleration Techniques Used in Unstructured Algorithms in the Solution of Aeronautical Problems – Part I, *Proceedings of the XVIII International Congress of Mechanical Engineering (XVIII COBEM)*, Ouro Preto, MG, Brazil, 2005.

[13] E. S. G. Maciel, Analysis of Convergence Acceleration Techniques Used in Unstructured Algorithms in the Solution of Aerospace Problems – Part II, *Proceedings of the XII Brazilian Congress of Thermal Engineering and Sciences (XII ENCIT)*, Belo Horizonte, MG, Brazil, 2008.

[14] E. S. G. Maciel, Comparison Among Structured First Order Algorithms in the Solution of the Euler Equations in Two-Dimensions, JBSMSE – Journal of the Brazilian Society of Mechanical Sciences and Engineering, Brazil, Vol. XXIX, No. 4, 2007, pp. 420-430.

[15] E. S. G. Maciel, Comparação Entre Algoritmos de Separação de Vetores de Fluxo e de Diferenças de Fluxo de Primeira Ordem na Solução das Equações de Euler em Duas Dimensões – Teoria, Proceedings of the Primer Congreso Argentino de Ingeniería Mecánica (I CAIM), Bahía Blanca, Argentina, 2008.

[16] E. S. G. Maciel, Comparison Among the First Order Upwind Algorithms of Roe, of Steger and Warming, of Van Leer and of Chakravarthy and Osher in the Solution of the Euler Equations in 2D – Theory, Proceedings of the 8th Symposium of Computational Mechanics (VIII SIMMEC), Belo Horizonte, MG, Brazi, 2008.

[17] B. Van Leer, Flux-Vector Splitting for the Euler Equations, Proceedings of the 8th International Conference on Numerical Methods in Fluid Dynamics, E. Krause, Editor, *Lecture Notes in Physics*, Vol. 170, 1982, pp. 507-512, Springer-Verlag, Berlin.

[18] R. Radespiel, and N. Kroll, Accurate Flux Vector Splitting for Shocks and Shear Layers, *Journal of Computational Physics*, Vol. 121, 1995, pp. 66-78.

[19] B. Van Leer, Towards the Ultimate Conservative Difference Scheme. II. Monotonicity and Conservation Combined in a Second-Order Scheme, *Journal of Computational Physics*, Vol. 14, 1974, pp. 361-370.

[20] P. L. Roe, In *Proceedings of the AMS-SIAM Summer Seminar on Large-Scale Computation in Fluid Mechanics*, Edited by B. E. Engquist et al., Lectures in Applied Mathematics, Vol. 22, 1983, p. 163.

[21] E. S. G. Maciel, Roe and Van Leer TVD Algorithms and Implicit Formulations Applied to the Euler Equations in Two-Dimensions, *Wseas Transactions on Applied and Theoretical Mechanmics*, 2012 (under review).

[22] E. S. G. Maciel, Comparison Between the Yee, Warming and Harten and the Hughson and Beran High Resolution Algorithms in the Solution of the Euler Equations in Two-Dimensions – Theory, *Proceedings of the XXVII Iberian Latin-American Congress on Computational Methods in Engineering (XXVII CILAMCE)*, Belém, PA, Brazil, 2006.

[23] H. C. Yee, R. F. Warming, and A. Harten, Implicit Total Variation Diminishing (TVD) Schemes for Steady-State Calculations, *Journal of Computational Physics*, Vol. 57, 1985, pp. 327-360.

[24] A. Jameson, and D. J. Mavriplis, Finite Volume Solution of the Two-Dimensional Euler Equations on a Regular Triangular Mesh, AIAA Journal, Vol. 24, No. 4, 1986, pp. 611-618.

[25] E. S. G. Maciel, *Simulação Numérica de Escoamentos Supersônicos e Hipersônicos Utilizando Técnicas de Dinâmica dos Fluidos Computacional*, PhD thesis, ITA, CTA, São José dos Campos, SP, Brazil, 258 p., 2002.

[26] J. D. Anderson Jr., *Fundamentals of Aerodynamics*, McGraw-Hill, Inc., EUA, 563p., 1984.